Dalton Transactions

ROYAL SOCIETY OF CHEMISTRY

PAPER

View Article Online
View Journal | View Issue

Cite this: *Dalton Trans.*, 2020, **49**, 9362

$Y_4Be_{33}Pt_{16}$ – a non-centrosymmetric cage superconductor with multi-centre bonding in the framework†

Alfred Amon, ‡ Eteri Svanidze, Yurii Prots, Michael Nicklas, Ulrich Burkhardt, Alim Ormeci, Andreas Leithe-Jasper * and Yuri Grin

Received 15th April 2020,
Accepted 11th June 2020

DOI: 10.1039/d0dt01374a

rsc.li/dalton

The new ternary compound $Y_4Be_{33}Pt_{16}$ was prepared from elements by arc melting, and its crystal structure was determined from single-crystal X-ray diffraction data (space group $I\bar{4}3d$, a = 13.4849(3) Å). The material is the first representative of a new structure type of complex intermetallic compounds and reveals a cage-like crystal structure. Analysis of chemical bonding by means of the electron localizabilty approach indicates ionic interaction of yttrium with the rest of the crystal structure, characteristic for cage compounds, in particular for clathrates. In contrast to the mostly two-centre bonding in the framework of clathrates, the new compound is characterized by a multi-centre interaction within the framework, caused by the demand of the valence electrons in the system. The non-centrosymmetric material enters the superconducting state at T_C = 0.9 K.

Introduction

The diversity of intermetallic structures is fascinating. These compounds can have unit cells with one atom as in α-Po (Pearson symbol *cP*1) or with more than twenty thousand atoms as in $Ta_{9063}Al_{12827.56}Cu_{1244.05}$ (Pearson symbol *cF*23134).[1–3] The reasons for such complex behaviour are still under discussion. The compounds with crystal structures containing more than *ca.* 100 atoms in the unit cell are notated as complex metallic alloys (CMA) or complex intermetallic compounds.[4] One of the characteristic features for CMA (but not for all) is the presence of different types of crystallographic disorder in crystal structures, which *de facto* means the violation of the translational symmetry in the strict sense. Recently, this was shown on examples of *o*-$Al_{13}Co_4$ (*oP*102-x)[5] and ternary clathrate $Ba_{7.81}Ge_{40.67}Au_{5.33}$ (*cP*54-x)[6] by the combination of X-ray diffraction on single crystals with high-resolution transmission electron microscopy. One of the possible reasons for such complex behaviour may be the low valence electron concentration in these materials, which (i) does not allow to use traditional electron counting schemes for understanding the composition and the crystal structure, and (ii) leads to multi-centre atomic interactions in the structures, recently shown *e.g.* for $Be_{21}Pt_5$.[7] Intermetallic compounds with complex crystal structures often show unusual physical behaviours. Physics and chemistry of CMA are discussed on the basis of the complexity of their crystal structures, whereby the latter is considered to be the origin of some specific behaviour of these substances. For instance, the intermetallic clathrates reveal unusual functionality in heat transport as a kind of phonon filters with the mean free path of phonons 10–100 nm.[6,8,9]

From the position in the Periodic Table, beryllium contributes only two valence electrons for the formation of bonds, thus the compounds with high beryllium content should be a suitable field to search for new complex intermetallic materials. The recently described binary $Be_{21}Pt_5$ has a large unit cell with 416 atoms (*cF*416), but does not reveal any crystallographic disorder.[7] The information about the ternary compounds of Be with other metals is rather scarce in the literature.[10] Our initial phase diagram studies showed, that – despite the clear electronic demand – the *R*–Be–*T* systems are characterized by formation of several ternary compounds similar to the *R*–*E*–*T* systems with *R* being alkaline- or rare-earth metals, *E* – *p*-block elements, and *T* – late transition metals. In this work, we present crystal structure and bonding analysis of the new superconductor $Y_4Be_{33}Pt_{16}$.

Results and discussion

The powder X-ray diffraction pattern of $Y_4Be_{33}Pt_{16}$, shown in Fig. 1, was indexed using a cubic cell with a = 13.4849(3) Å. The structure was solved and refined from single-crystal diffr-

Max-Planck-Institut für Chemische Physik fester Stoffe, Nöthnitzer Straße 40, Dresden 01187, Germany

†Electronic supplementary information (ESI) available. CCDC 1996617. For ESI and crystallographic data in CIF or other electronic format see DOI: 10.1039/d0dt01374a

‡Current address: Department of Chemistry, University College London.

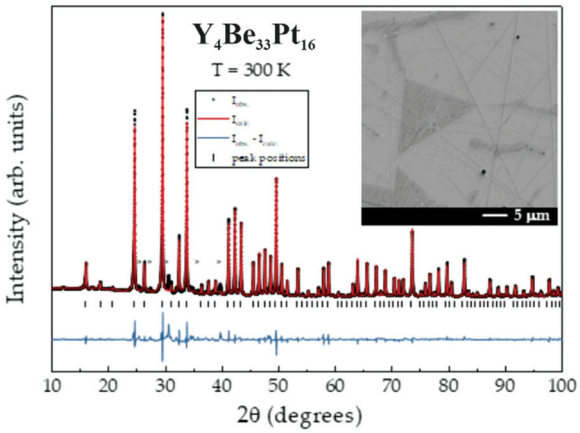

Fig. 1 X-ray powder diffraction pattern for $Y_4Be_{33}Pt_{16}$. Reflections of the minority phases ($Be_{21}Pt_5$, Y, and Pt) are marked by asterisks. Inset: Microstructure (material contrast image, SEM) shows the Y- and Pt-containing majority phase (light gray) and the Pt-poor minority phase (dark gray).

Table 1 Crystallographic data for $Y_4Be_{33}Pt_{16}$ (single-crystal diffraction experiment)

Crystal system	Cubic
Composition	$Y_4Be_{33}Pt_{16}$
Space group	$I\bar{4}3d$
Pearson symbol	$cI212$
Formula units per u. c. Z	4
Unit cell parameter a	13.4849(3) Å[a]
Unit cell volume V	2452.1(2) Å^3
Calculated density	10.22 g cm^{-3}
Radiation, wavelength	MoK_a, 0.71073 Å
Absorption coefficient	105.2 mm^{-1}
Diffraction system	Rigaku AFC7
$2\theta_{max}$	86.2°
$N(hkl)$ measured	27 218
$N(hkl)$ unique	1477
$N(hkl)$ observed	1446
R_{int}; R_s	0.045; 0.032
Refined parameters	28
R_F; wR_F^2	0.044; 0.088
Weighting scheme	$w_i = [\ln(F_{obs,i}^4)]^{-1}$
Extinction coefficient[17]	0.000062(9)
Flack parameter	−0.005(10)
Residual electron density max; min	+2.3; −1.9 e Å^{-3}

[a] Lattice parameter refined from the X-ray powder diffraction data ($CuK_{\alpha1}$ radiation).

action data in the non-centrosymmetric space group $I\bar{4}3d$. The main crystallographic information is presented in Table 1, the atomic coordinates and isotropic atomic displacement parameters are shown in Table 2, the anisotropic displacement parameters for Y and Pt atoms as well as the interatomic distances are listed in ESI (Tables S1 and S2,† respectively).

The atoms in the crystal structure of $Y_4Be_{33}Pt_{16}$ reveal coordination polyhedrons characteristic for intermetallic compounds in the ternary systems of rare-earth and related metals as R component with transition metals and p-block elements. The yttrium atoms are located within a spacious polyhedron with 20 vertices, being very similar to that of Ca in the $CaCu_5$

Table 2 Atomic coordinates and displacement parameters for $Y_4Be_{33}Pt_{16}$

Atom	Site	x/a	y/b	z/c	$B_{eq/iso}$ [a] (Å^{-2})
Y	16c	0.8097(1)	x	x	0.66(2)
Pt1	16c	0.93652(4)	x	x	0.594(6)
Pt2	48e	0.48917(4)	0.89865(4)	0.77608(4)	0.607(8)
Be1	12a	$\frac{5}{8}$	0	$\frac{3}{4}$	1.2(6)
Be2	24d	0.914(3)	0	$\frac{1}{4}$	1.1(4)
Be3	48e	0.056(2)	0.989(2)	0.664(2)	1.1(3)
Be4	48e	0.620(2)	0.919(2)	0.893(2)	1.0(3)

[a] $B_{eq} = \frac{1}{3}[B_{11} \times a^{*2} \times a^2 + \cdots + 2B_{23} \times b^* \times c^* \times b \times c \times \cos(\alpha)]$.

structure type and its several derivatives[11,12] (Fig. 2, top panel). Interestingly, there are three additional Be1 ligands at the distance of 3.666 Å, which is much longer than other yttrium contacts (Table S2†) and – from distance analysis – these three do not necessarily belong to the first coordination sphere (*cf.* analysis of chemical bonding below). While the platinum atoms have environments derived from the Frank–Kasper polyhedrons with coordination numbers of CN(Pt1) = 14 and CN(Pt2) = 13, Be1 has a bisdisphenoid-like environment with eight closer neighbours (and additional four yttrium species at a much longer distance), all remaining beryllium species have 12 or 13 ligands with their coordination environments derived from an icosahedron (Fig. 2, top panel).

The crystal structure of $Y_4Be_{33}Pt_{16}$ can be visualized by considering the coordination environment of yttrium. Adjacent coordination polyhedrons of Y are vertex-sharing *via* the Pt1 position. This results in the formation of a linear rod-like arrangement of interpenetrating Y and Pt1 polyhedrons, as shown in Fig. 2 (middle panel), along the three-fold axes of the cubic unit cell ({111} directions). The resultant rod packing is presented in Fig. 2 (bottom panel) and was first described as crystallographic object in ref. 13. The existence of voids between the rods is due to an incomplete space filling. These voids are located at $(\frac{7}{8}\ 0\ \frac{1}{4})$ (Wyckoff site 12*b*) and $(\frac{3}{8}\ 0\ \frac{1}{4})$ (Wyckoff site 12*a*). The former are empty in $Y_4Be_{33}Pt_{16}$, as they are too small to contain an atom. The voids located at $(\frac{3}{8}\ 0\ \frac{1}{4})$ having the shape of a bisdisphenoid are occupied by Be1.

Among the $CaCu_5$ derivatives, the crystal structure of $Y_4Be_{33}Pt_{16}$ is closely related to the ferromagnet $Nd_2Fe_{23}B_3$ (space group $I\bar{4}3d$, a = 14.19 Å).[14–16] For a comparison, the compositions can be written as $Nd_4Fe_{30}(B_2)_3Fe_{16}$ and $Y_4Be_{30}Be_3Pt_{16}$. In the $Nd_2Fe_{23}B_3$ structure, the Y site is occupied by Nd, all other positions beside Be1 – by iron. While the bisdisphenoid in $Y_4Be_{33}Pt_{16}$ is occupied by a single Be1 atom (Wyckoff site 12a), the same coordination environment is occupied in $Nd_2Fe_{23}B_3$ by a B_2 pair with the centre at the 12a site (Fig. S1†). In this way, the B atoms belong to the coordination sphere of Nd with d(B1–Nd1) = 3.32 Å in $Nd_2Fe_{23}B_3$, in contrast to Be1 in $Y_4Be_{33}Pt_{16}$ which shows much longer distance of d(Be1–Y) = 3.666 Å.

The complex intermetallic structures with large cubic unit cell, in particular derivatives of the gamma-brass structural pattern, can often be interpreted from the crystallographic

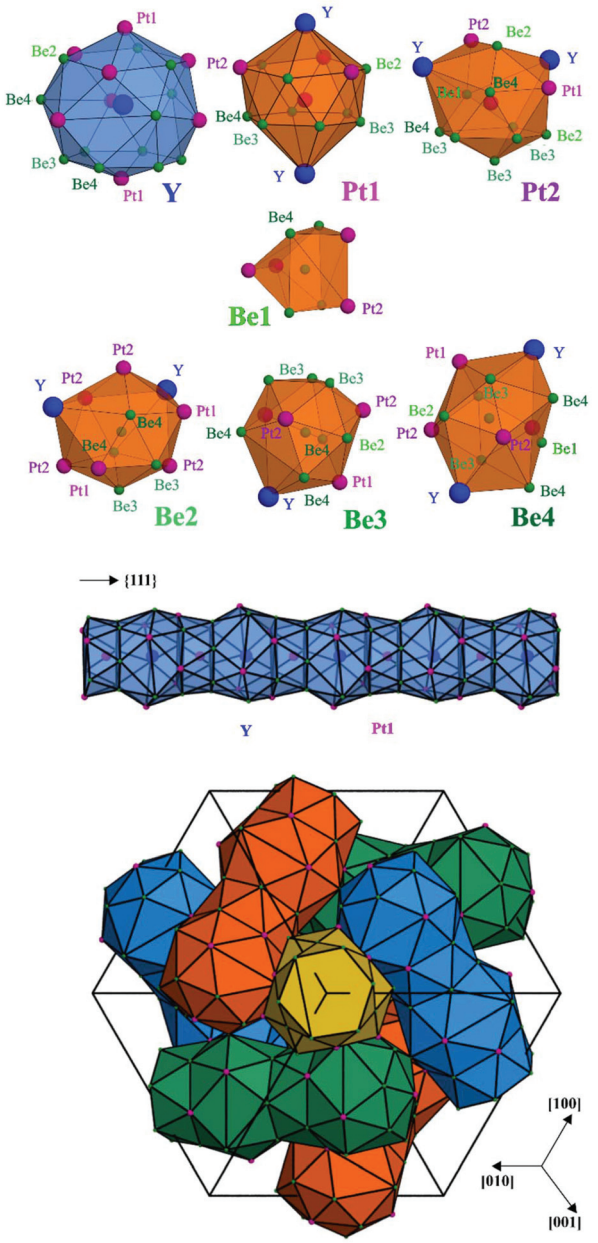

Fig. 2 Crystal structure of $Y_4Be_{33}Pt_{16}$ with the Y, Pt, and Be atoms represented by blue, pink, and green spheres, respectively: (top) coordination polyhedrons of atoms as obtained from analysis of interatomic distances; (middle) interpenetrating polyhedrons of Y and Pt1 along the three-fold axes; (bottom) rod packing of the interpenetrating polyhedron arrangements in the unit cell, the different colours visualize rods on different three-fold axes.

point of view as packings of nested polyhedrons.[18] Recently, this was explained on example of $Be_{21}Pt_5$ by the formation of multi-atomic bonding interactions centred at the middle points of the nested polyhedrons.[7] Interestingly, this approach does not work reasonably well for $Y_4Be_{33}Pt_{16}$. This observation was the starting point for the analysis of chemical bonding in $Y_4Be_{33}Pt_{16}$ employing the electron localizability approach.

As for most intermetallic beryllium compounds, a characteristic feature of $Y_4Be_{33}Pt_{16}$ is the very low valence electron concentration (VEC) of *ca.* 1.4 e per atom, which is even lower than in the gamma-brass derivative $Be_{21}Pt_5$ (1.62 e per atom). An important factor stabilizing the latter structure was found to be the charge transfer from Be to Pt.[7] In order to study the role of the ionic contributions to the bonding, the electron density in $Y_4Be_{33}Pt_{16}$ was investigated applying the QTAIM (Quantum Theory of Atoms In Molecules[19]) approach. The zero-flux surfaces in the distribution of electron density define the shape of the atoms in the QTAIM representation. Integration of electron density within the atomic shapes yields their electronic populations and effective charges (Fig. 3). The yttrium atoms in $Y_4Be_{33}Pt_{16}$ in the QTAIM representation have a shape close to a spherical one, which is characteristic for cage compounds, *e.g.* clathrates of Ba or Sr.[9,20] Their effective charge of +1.70 is also characteristic for the earth-alkaline and rare-earth atoms in intermetallic clathrates.[20,21] The shapes of the QTAIM atoms of platinum and beryllium are far from a sphere. They have closer to plane or even concave faces. While beryllium atoms – as expected from the electronegativity differences – reveal positive effective charges between +1.30 and +1.40, the platinum species have large negative charges of −2.72 and −3.31 for Pt1 and Pt2, respectively. This confirms strong charge transfer in the compound according to the scheme $[Y^{+1.70}]_4[Be1^{+1.36}]_3[Be2^{+1.30}]_6[Be3^{+1.36}]_{12}[Be4^{+1.31}]_{12}[Pt1^{-2.72}]_4[Pt2^{-3.31}]_{12}$.

Further information about atomic interactions was obtained by applying the electron localizability approach. The distribution of the electron localizability indicator (ELI-D) in the vicinity of the yttrium nuclei is close to a spherical one, whereby the valence shell (4^{th}) is absent. The light structuring of the penultimate shell indicates the participation of the elec-

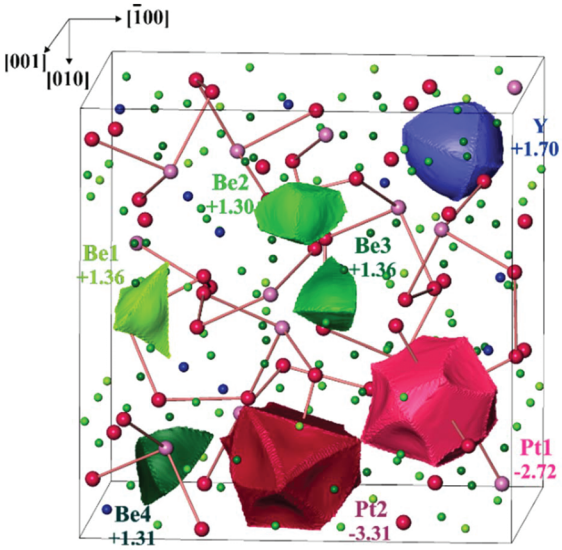

Fig. 3 QTAIM atoms and their effective charges in $Y_4Be_{33}Pt_{16}$. The Pt–Pt contacts with 2.82 Å < *d*(Pt–Pt) < 2.91 Å are shown to emphasize the volume representation.

trons from this shell in the bonding. The intersection with the QTAIM yttrium atom reveals that the latter bears only the inner shells, confirming the ionic interaction of yttrium with the Be–Pt framework (Fig. 4, top panel). In the cage wall, there are two bonds involving Be2, Be4 and Pt2. Populations are 1.63 and 1.36 electrons, respectively. The interesting aspect is that Pt1 also contributes to them. Its contribution is comparable to those of Be2 and Be4. Hence, each attractor describes a four-atomic bond, two Pt and two Be. This reflects the characteristic multi-atomic interaction in the whole Be–Pt framework. The distribution of ELI-D in the (Be1–Pt2–Be4) triangle reveals one maximum located within the triangle. The intersection of the ELI-D basin of this maximum with the QTAIM shapes of the neighbouring atoms (Fig. 4, middle panel) shows the Be1, Be4, and Pt2 atoms contributing 0.11, 0.15, and 1.45 of the total population of 1.84 electrons for this basin. This confirms the mainly three-atomic (3a) character of the interaction in this part of the structure. The remaining 0.13 electrons originate from two other Pt2, one Be3, and even one yttrium neighbours, suggesting that even more atoms are participating in this multi-atomic bonding. The Pt atoms contribute the majority of the population for the bonding basins, which makes the multi-centre interactions strongly polar. The bonding analysis reveals that the Be1 atoms should be included into the coordination sphere of yttrium despite a large interatomic distance (*cf.* distance-based considerations above and comparison of the Y-polyhedrons in Fig. S1(e)†). The Y-centred cages – as obtained from the bonding analysis – within the three-dimensional Be–Pt framework fill-up the large part of the unit cell of $Y_4Be_{33}Pt_{16}$ (Fig. 4, bottom panel). In summary, analysis of the chemical bonding classifies $Y_4Be_{33}Pt_{16}$ as a cage compound, *e.g.* a material with its crystal structure in the form of a 3D framework with large cages. Ionic interaction of cationic yttrium species in the cages of the anionic Be–Pt framework is the bonding characteristic of this cage structure. In contrast to other representatives of cage compounds, *e.g.* intermetallic clathrates with mainly two-centre (non-polar or polar) bonds in the framework, the framework in $Y_8Be_{66}Pt_{32}$ is formed by multi-atomic (polar) interaction. In agreement with the chemical bonding picture, the calculated electronic density of states of $Y_4Be_{33}Pt_{16}$ is characterized by the intermixing of Pt and Be states in the whole energy range and shows three main regions (Fig. 5). The low-energy range ($E < -6.7$ eV) is formed mainly by the *s* states of Be and Pt with small contributions of the *s* states of yttrium, reflecting the bonding in the Be–Pt framework. The middle-energy region (-6.7 eV $< E < -2.3$ eV) is dominated by *d* states of platinum atoms. The region below the Fermi level (E_F) contains contributions of all essential atomic states. Interestingly, a pseudo gap is found above the Fermi level (due to the band dispersion along Γ–H in the Brillouin zone, Fig. S2†), in contrast to the typical DOS distribution in cage compounds with two-centre bonds in the framework, where the pseudo gap appears typically close to E_F.[9] The presence of non-filled states agrees with the electron-deficient situation in this material.

The non-centrosymmetric compound $Y_4Be_{33}Pt_{16}$ enters a superconducting state below T_C = 0.9 K, as evidenced by the BCS-like anomaly observed in specific heat data, shown in Fig. 6. A fit to the specific heat data above the superconducting transition (dashed line), can be used to estimate the value of

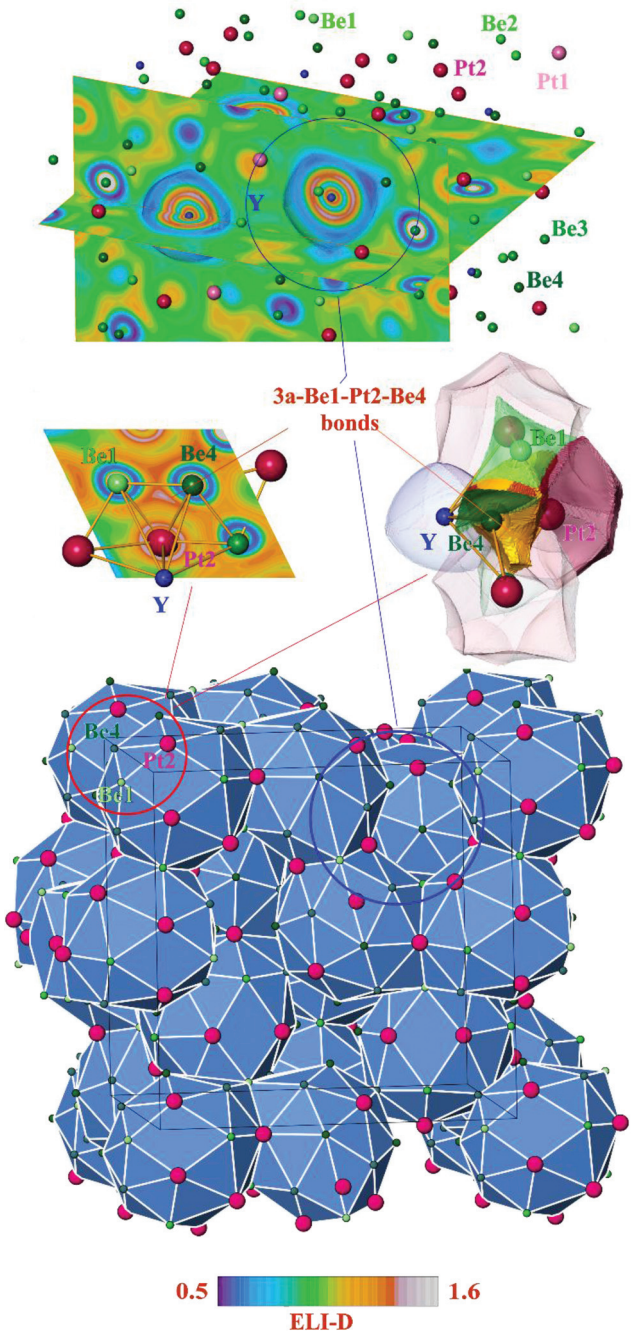

Fig. 4 Atomic interactions in $Y_4Be_{33}Pt_{16}$ by electron localizability approach: (top panel) distribution of the ELI-D in the plane crossing two neighbouring yttrium atoms; (middle left panel) distribution of ELI-D in one of the face planes of the coordination polyhedron of yttrium with the Pt2, Be1 and Be4 atoms; (middle right panel) bonding basin of the three-atomic interaction Pt2–Be1–Be4 (yellow bulk) intersected by the QTAIM atomic basins of the participating atoms (transparent), three main contributing atoms are labelled; (bottom panel) crystal structure of $Y_4Be_{33}Pt_{16}$ as a packing of the coordination polyhedrons of Y (blue) as obtained from the bonding analysis.

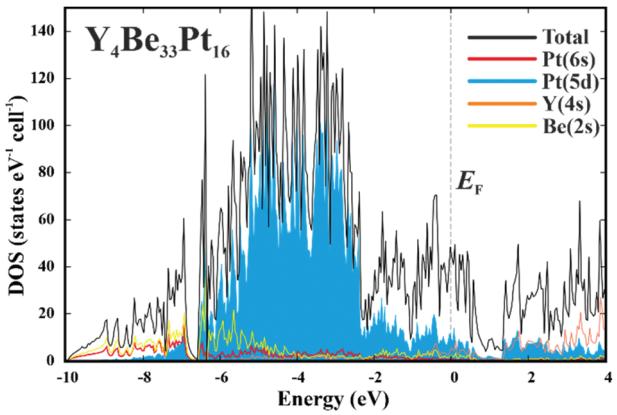

Fig. 5 Calculated electronic density of states (DOS) for $Y_4Be_{33}Pt_{16}$. The total DOS (black line) is shown together with the contributions of essential atomic states.

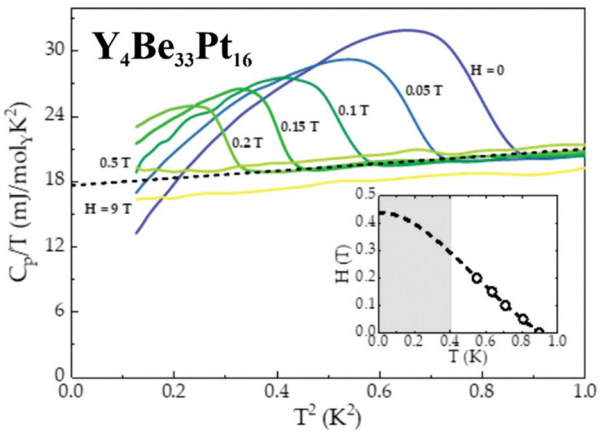

Fig. 6 Superconducting properties of $Y_4Be_{33}Pt_{16}$: specific heat data, scaled by temperature T, C_P/T as a function of T^2 in applied magnetic fields $0 \leq H \leq 9$ T. The dashed line represents a fit from which the value of γ_n was extracted. Inset: H–T phase diagram for $Y_4Be_{33}Pt_{16}$ with the values of $H_{c2}(T)$ taken from specific heat data.

the normal state electronic specific heat coefficient $\gamma_n = 18$ mJ mol_Y^{-1} K^{-2}, as well as cubic term coefficient $\beta = 4.5$ mJ mol_Y^{-1} K^{-3}. Using the value of γ_n, it is then possible to estimate the effective mass m^* from the following relation:[22] $m^* = (\gamma_n \hbar^2 k_F^2)/(\pi^2 n k_B^2) \approx m_e$, indicating lack of electron mass enhancement (equivalently, the theoretically computed value of DOS at the Fermi energy yields $\gamma_{calc} = 16.3$ mJ mol_Y^{-1} K^{-2}). From the value of β, the Debye temperature θ_D can be calculated using $\theta_D = [(14\pi^4 N_A r k_B)/(5\beta)]^{1/3} = 358$ K.[22] Consequently, the value of θ_D can then be used to estimate the strength of the electron–phonon coupling, employing the McMillan's formula.[23] Typically, materials with $\lambda_{e-p} \rightarrow 1$ are classified as strongly-coupled superconductors, while $\lambda_{e-p} \rightarrow 0.5$ indicates weak coupling.[23] For $Y_4Be_{33}Pt_{16}$, $0.38 \leq \lambda_{e-p} \leq 0.47$, indicating weakly-coupled superconductivity. Once the phonon contribution to the specific heat (βT^3) has been subtracted from the specific heat data, an entropy conserving construction (not shown) yields the ratio $\Delta C_e/\gamma_n T_C \approx 1.80$, which is comparable to the BCS value of $\Delta C_e/\gamma_n T_C = 1.44$, consistent with $Y_4Be_{33}Pt_{16}$ being a weakly-coupled superconductor. As expected, the critical temperature T_C is gradually suppressed by the application of a magnetic field, consistent with type-II superconductivity, allowing to construct the H–T phase diagram (inset of Fig. 6). A relatively small value of the upper critical field $H_{c2} = 0.44$ T, extracted from a Ginzburg–Landau fit[22] (dashed line), further confirms weak coupling in $Y_4Be_{33}Pt_{16}$. The upper critical fields of non-centrosymmetric superconductors are often rather high (on the order of several or even dozens of Tesla), but $Y_4Be_{33}Pt_{16}$ belongs to the smaller family of non-centrosymmetric superconductors with the upper critical fields on the order of few hundred Oersted. The other examples are AuBe ($H_{c2} = 335$ Oe),[24] Mo_2Al_3C ($H_{c2} = 50$ Oe),[25] or $LaRhSi_3$ ($H_{c2} = 180$ Oe).[26]

The fact, that – despite of absence of inversion symmetry – no distinct deviations from BCS theory are observed, points towards the lack of strong correlation effects.[27,28] However, a more comprehensive analysis of the superconducting state in $Y_4Be_{33}Pt_{16}$ is currently underway. In particular, because several in-depth muon spin-rotation, relaxation, and resonance experiments performed on another Be-containing non-centrosymmetric superconductor BeAu[24] revealed that not only type-I character,[29] but also a multi-gap nature of superconductivity[30] may exist in such unconventional systems.

Experimental

Synthetic procedures

All sample preparation was performed in a laboratory specialized for work with Be, inside a argon-atmosphere glove box system (MBraun, $p(H_2O/O_2) < 0.1$ ppm).

Caution! Beryllium is considered (according to UN GHS criteria) a health risk and experiments require appropriate infra structure.

Polycrystalline samples around the composition $Y_4Be_{33}Pt_{16}$ were synthesized by arc melting Y (pieces, Ames, >99.9%), Pt (foil, Chempur, >99.9%), and Be (sheet, Heraeus, >99.9%) in the 10 : 30 : 60 ratio. The samples did not exhibit any marked air or moisture sensitivity. Small amounts of impurities were found to be present in all samples. The minority phases are $Be_{21}Pt_5$ (superconductor with $T_C = 2.06$ K (ref. 7)), Be_5Pt (semiconductor[31]), as well as elemental Pt in the amount of <3%. Temperature treatment, as well as slight variation of the initial composition did not result in an improved sample quality.

Crystallography

Powder X-ray diffraction was performed on a Huber G670 Image plate Guinier camera with a Ge-monochromator ($CuK_{\alpha 1}$ radiation, $\lambda = 1.54056$ Å). Phase identification was done using the WinXPow software.[32] All crystallographic calculations were done with the WinCSD software package[33] Single-crystal X-ray diffraction data have been collected on a Rigaku AFC7 diffract-

ometer equipped with a Saturn 724 + CCD detector using MoK_α radiation (λ = 0.71073 Å).

Chemical analysis

Chemical composition of polished samples was studied using energy-dispersive X-ray spectroscopy (EDS) with an UltraDry EDS detector (ThermoFisher NSS7) attached to a Jeol JSM 6610 scanning electron microscope (SEM). The semi-quantitative analysis was performed with 25 keV acceleration voltage and ≈3 nA beam current.

Physical properties measurements

Heat capacity was measured in the temperature range from 0.4 K to 10 K, in magnetic fields up to H = 9 T using a QD Physical Property Measurement System.

Calculation procedures

Electronic structure calculations were performed by using the all-electron, full-potential local orbital (FPLO) method.[34] All main results were obtained within the local density approximation (LDA) to the density functional theory through the Perdew–Wang parametrization for the exchange–correlation effects.[35] Application of the generalized gradient approximation did not reveal essential differences in the electronic structure below and in vicinity of the Fermi level. Chemical bonding analysis in position space was performed within the approach of combined topological analysis of electron density (ED) and electron localizability indicator (ELI). The former type of analysis forms the basis of the quantum theory of atoms in molecules (QTAIM).[19] ELI was calculated in the ELI-D representation[36–38] by a module implemented in the FPLO package.[39] Topological analysis of the ED and the ELI-D were carried out by the program DGrid.[40]

Conclusions

The ternary compound $Y_4Be_{33}Pt_{16}$ is the first representative of a new prototype of intermetallic cage compounds with an unusual combination of structural and bonding features. The cubic crystal structure with 212 atoms in the unit cell is – in contrast to many other complex intermetallic structures – completely ordered and does not show violation of the translational symmetry, characteristic for CMA materials. Analysis of chemical bonding in position space reveals mainly ionic interaction of Y with the remaining parts of the structure, indicating an analogy to intermetallic clathrates and classifying the new atomic arrangement as a cage-like one. In contrast to other cage materials – clathrates – with mainly two-centre bonding in the framework, the framework atoms in $Y_4Be_{33}Pt_{16}$ participate only in multi-centre interactions. On top of the interesting structure-bonding relationship, the new compound is a non-centrosymmetric BCS-type superconductor with T_C = 0.9 K.

Conflicts of interest

There are no conflicts of interest.

Acknowledgements

The authors acknowledge W. Schnelle for valuable discussions, H. Borrmann and S. Hückmann for assistance in powder diffraction experiments, K. Vanatko and R. Gellrich for support of preparative work. Open Access funding provided by the Max Planck Society.

References

1 R. J. de Sando and R. C. Lange, *J. Inorg. Nucl. Chem.*, 1966, **28**, 1837.
2 T. Weber, J. Dshemuchadse, M. Kobas, M. Conrad, B. Harbrecht and W. Steurer, *Acta Crystallogr., Sect. B: Struct. Sci.*, 2009, **65**, 308.
3 Yu. Grin, in *Comprehensive Inorganic Chemistry II*, Elsevier, Oxford, 2013, vol. 2, p. 359.
4 *Complex Metallic Alloys Fundamentals and Applications*, ed. J.-M. Dubois and E. Belin-Ferré, Wiley-VCH, Weinheim, 2011.
5 P. Simon, I. Zelenina, R. Ramlau, W. Carrillo-Cabrera, U. Burkhardt, H. Borrmann, R. Cardoso Gil, M. Feuerbacher, P. Gille and Yu. Grin, *J. Alloys Compd.*, 2020, **820**, 153363.
6 P. F. Lory, S. Pailhès, V. M. Giordano, H. Euchner, H. D. Nguyen, R. Ramlau, H. Borrmann, M. Schmidt, M. Baitinger, M. Ikeda, P. Tomeš, M. Mihalkovič, C. Allio, M. R. Johnson, H. Schober, Y. Sidis, F. Boudarot, L. P. Regnault, J. Ollivier, S. Paschen, Yu. Grin and M. de Boissieu, *Nat. Commun.*, 2017, **8**, 1.
7 A. Amon, A. Ormeci, M. Bobnar, L. G. Akselrud, M. Avdeev, R. Gumeniuk, U. Burkhardt, Yu. Prots, C. Hennig, A. Leithe-Jasper and Yu. Grin, *Acc. Chem. Res.*, 2018, **51**, 214.
8 H. Euchner, S. Pailhès, L. T. Nguyen, W. Assmus, F. Ritter, A. Haghighirad, Yu. Grin, S. Paschen and M. de Boissieu, *Phys. Rev. B: Condens. Matter Mater. Phys.*, 2012, **86**, 224303.
9 H. Zhang, H. Borrmann, N. Oeschler, C. Candolfi, W. Schnelle, M. Schmidt, U. Burkhardt, M. Baitinger, J.-T. Zhao and Yu. Grin, *Inorg. Chem.*, 2011, **50**, 1250.
10 O. Janka and R. Pöttgen, *Z. Naturforsch., B: J. Chem. Sci.*, 2020, **75**, 143.
11 W. B. Pearson, *The crystal Chemistry and Physics of metals and Alloys*, Wiley-Interscience, N.Y., 1972, p. 643.
12 P. I. Krypiakevich, *Structure Types of Intermetallic Compounds*, Nauka, Moscow, 1977 (in Russian).
13 M. O'Keeffe and S. Andersson, *Acta Crystallogr., Sect. A: Cryst. Phys., Diffr., Theor. Gen. Crystallogr.*, 1977, **33**, 914.
14 K. H. Buschow, D. B. de Mooij and H. M. van Noort, *J. Less-Common Met.*, 1986, **125**, 135.

15 D. de Mooij and K. H. J. Buschow, *Philips J. Res.*, 1986, **41**, 400.
16 C. Gou, Z. X. Cheng, D. F. Chen, S. W. Niu, Q. W. Yan, P. L. Zhang, B. G. Shen and L. Y. Yang, *J. Magn. Magn. Mater.*, 1993, **128**, 26.
17 G. M. Sheldrick, *Acta Crystallogr., Sect. A: Found. Crystallogr.*, 2008, **64**, 112.
18 B. Chabot, K. Cenzual and E. Parthé, *Acta Crystallogr., Sect. A: Cryst. Phys., Diffr., Theor. Gen. Crystallogr.*, 1981, **37**, 6.
19 R. F. W. Bader, *Atoms in Molecules: A Quantum Theory*, Oxford University Press, Clarendon Press, 1994.
20 J. Hübner, Yu. Prots, W. Schnelle, M. Bobnar, M. König, M. Baitinger, P. Simon, W. Carrillo-Cabrera, A. Ormeci, E. Svanidze, Yu. Grin and U. Schwarz, *Chem. – Eur. J.*, 2020, **26**, 756.
21 A. Ormeci and Yu. Grin, *J. Thermoelectr.*, 2015, **6**, 16.
22 M. Tinkham, *Introduction to Superconductivity*, McGraw-Hill, New York, 1996.
23 W. L. McMillan, *Phys. Rev.*, 1968, **167**, 331.
24 A. Amon, E. Svanidze, R. Cardoso-Gil, M. N. Wilson, H. Rosner, M. Bobnar, W. Schnelle, J. W. Lynn, R. Gumeniuk, C. Hennig, G. M. Luke, H. Borrmann, A. Leithe-Jasper and Yu. Grin, *Phys. Rev. B*, 2018, **97**, 014501.
25 A. B. Karki, Y. M. Xiong, I. Vekhter, D. Browne, P. W. Adams, D. P. Young, K. R. Thomas, J. Y. Chan, H. Kim and R. Prozorow, *Phys. Rev. B: Condens. Matter Mater. Phys.*, 2010, **82**, 064512.
26 N. Kimura, H. Ogi, K. Satoh, G. Ohsaki, K. Saitoh, H. Iida and H. Aoki, *JPS Conf. Proc.*, 2014, **3**, 015011.
27 Non-centrosymmetric superconductors, *Lecture Notes in Physics*, ed. E. Bauer and M. Sigrist, 2012, vol. 847, p. 3.
28 F. Kneidinger, E. Bauer, I. Zeiringer, P. Rogl, C. Blaas-Schenner, D. Reith and R. Podloucky, *Phys. C*, 2015, **514**, 388.
29 J. Beare, M. Nugent, M. N. Wilson, Y. Cai, T. J. S. Munsie, A. Amon, A. Leithe-Jasper, Z. Gong, S. L. Guo, Z. Guguchia, Yu. Grin, Y. J. Uemura, E. Svanidze and G. M. Luke, *Phys. Rev. B*, 2019, **99**, 134510.
30 R. Khasanov, R. Gupta, D. Das, A. Amon, A. Leithe-Jasper and E. Svanidze, *Phys. Rev. Res.*, 2020, **2**, 023142.
31 A. Amon, E. Svanidze, A. Ormeci, M. König, D. Kasinathan, D. Takegami, Yu. Prots, Y. F. Liao, K. D. Tsuei, L. H. Tjeng, A. Leithe-Jasper and Yu. Grin, *Angew. Chem., Int. Ed.*, 2019, **58**, 15928.
32 *STOE Powder Diffraction Software WinXPow (version 2)*, STOE and Cie GmbH, Darmstadt, 2001.
33 L. Akselrud and Yu. Grin, *J. Appl. Crystallogr.*, 2014, **47**, 803.
34 K. Koepernik and H. Eschrig, *Phys. Rev. B: Condens. Matter Mater. Phys.*, 1999, **59**, 1743.
35 J. P. Perdew and Y. Wang, *Phys. Rev. B: Condens. Matter Mater. Phys.*, 1992, **45**, 13244.
36 M. Kohout, *Int. J. Quantum Chem.*, 2004, **97**, 651.
37 M. Kohout, F. R. Wagner and Yu. Grin, *Int. J. Quantum Chem.*, 2006, **106**, 1499.
38 M. Kohout, *Faraday Discuss.*, 2007, **135**, 43.
39 A. Ormeci, H. Rosner, F. R. Wagner, M. Kohout and Yu. Grin, *J. Phys. Chem. A*, 2006, **110**, 1100.
40 M. Kohout, *DGrid, version 4.6*, Radebeul, 2011.